International Journal of Heat and Mass Transfer 52 (2009) 2042–2048

Contents lists available at ScienceDirect

International Journal of Heat and Mass Transfer

journal homepage: www.elsevier.com/locate/ijhmt

Laminar convective heat transfer and viscous pressure loss of alumina–water and zirconia–water nanofluids

Ulzie Rea, Tom McKrell, Lin-wen Hu *, Jacopo Buongiorno

Massachusetts Institute of Technology, 77 Massachusetts Avenue, Cambridge, MA 02139, USA

ARTICLE INFO

Article history:
Received 11 April 2008
Received in revised form 23 October 2008
Available online 26 December 2008

Keywords:
Nanofluids
Nanoparticle colloids
Laminar flow
Heat transfer enhancement

ABSTRACT

Laminar convective heat transfer and viscous pressure loss were investigated for alumina–water and zirconia–water nanofluids in a flow loop with a vertical heated tube. The heat transfer coefficients in the entrance region and in the fully developed region are found to increase by 17% and 27%, respectively, for alumina–water nanofluid at 6 vol % with respect to pure water. The zirconia–water nanofluid heat transfer coefficient increases by approximately 2% in the entrance region and 3% in the fully developed region at 1.32 vol %. The measured pressure loss for the nanofluids is in general much higher than for pure water. However, both the measured nanofluid heat transfer coefficient and pressure loss are in good agreement with the traditional model predictions for laminar flow, provided that the loading- and temperature-dependent thermophysical properties of the nanofluids are utilized in the evaluation of the dimensionless numbers. In other words, no abnormal heat transfer enhancement or pressure loss was observed within measurement errors.

1. Introduction

Heat transfer enhancement through modification of fluid thermophysical properties by adding dispersed particles to a base fluid has been a topic of interest since the early works by Ahuja [1] and Liu et al. [2]. However, the engineering applicability of micron-sized particle colloids is generally hindered by sedimentation and erosion. Nanofluids, colloidal dispersions of nano-sized particles in a based fluid, have been shown to maintain stability through the use of surfactant and pH control. The experimental studies of Masuda et al. [3], Choi [4], Eastman et al. [5], Choi et al. [6], Assael et al. [7], among others, have reported significant enhancement of nanofluid thermal conductivity, beyond the predictions of classical heterogeneous mixed media models such as Maxwell-Garnett [8] and Hamilton and Crosser [9]. This finding generated great interest in nanofluids and their potential for heat transfer enhancement.

Several experimental studies on nanofluid single-phase heat transfer have been reported in the literature. Pak and Cho [10] explored alumina–water and titania–water nanofluids in turbulent convective heat transfer in tubes. Xuan and Li [11] investigated turbulent convective heat transfer and flow features of copper oxide in water nanofluids. Xuan and Roetzel [12] considered a heat transfer correlation for nanofluids to capture the effect of energy transport by particle "dispersion". Yang et al. [13] measured laminar convective heat transfer performance of graphite nanofluids in horizontal circular tube. Wen and Ding [14] studied nanofluid laminar flow convective heat transfer and reported significant enhancement in the entry region. Ding et al. [15] observed significant convective heat transfer enhancement of multi-walled carbon nanotube dispersion in water and the enhancement depended on the flow conditions (Reynolds number), carbon nanotube concentration and pH. Heris et al. [16–17] studied the effects of alumina and copper oxide nanofluids on laminar heat transfer in a circular tube under constant wall temperature boundary condition. They reported heat transfer coefficient enhancement for both nanofluids with increasing nanoparticle concentrations as well as Peclet number, and observed higher enhancement in alumina nanofluid than copper oxide. He et al. [18] investigated the heat transfer of titania nanofluids in both laminar and turbulent flow, and found the heat transfer enhancement increased with particle concentration and decreasing particle size. Convective heat transfer of alumina nanofluid in microchannels was investigated by Lee et al. [19]. The effective thermal conductivity of 2 vol % nanofluids was found to increase by only 4–5% and the viscosity by 12% relative to the base fluid. Nanofluid application in microelectronics cooling were recently explored by Chein and Chuang [20] and Nguyen et al. [21].

Most of the nanofluid studies reported in the literature have concluded or assumed that nanofluids provide heat transfer enhancement with respect to their respective base fluids. Nonetheless, assessment of what constitutes an enhancement has not been determined on the same basis. An increased heat transfer coefficient may simply reflect the changes in the thermal physical prop-

* Corresponding author. Tel.: +1 617 258 5860.
E-mail address: lwhu@mit.edu (L.-w. Hu).

0017-9310/$ - see front matter © 2008 Elsevier Ltd. All rights reserved.
doi:10.1016/j.ijheatmasstransfer.2008.10.025

Nomenclature

c	specific heat, J/kg K
D	diameter, m
h	heat transfer coefficient, J/kg
k	thermal conductivity, W/m K
L	length, m
q''	heat flux, W/m^2
T	temperature, °C
V	velocity, m/s
w	weight percent
x	distance, m

Greek symbols

ϕ	nanoparticle volumetric fraction
μ	viscosity, Pa s
ρ	density, kg/m^3

Subscripts

f	fluid
p	nanoparticle

erties of the nanofluid being tested while the models and correlations developed for simple fluids still apply. As an example, a recent study in our group measured the convective heat transfer and pressure loss behavior of alumina–water and zirconia–water nanofluids in fully developed turbulent flow. The results indicated that the turbulent heat transfer and pressure loss can be predicted by means of the traditional correlations and models, as long as the measured temperature- and loading-dependent nanofluid properties are used in calculating the dimensionless numbers [22]. This study is expanded from our earlier work on turbulent flow and is aimed to investigate the heat transfer characteristics of the same nanofluids (alumina–water and zirconia–water) in the laminar flow regime. The key contribution of this work is in providing experimental data to demonstrate the hypothesis that the nanofluids can be treated as homogeneous mixtures, as such the heat transfer coefficient enhancement is not abnormal, but due to the different mixture properties of the nanofluids.

2. Experiment setup

A schematic of the experimental apparatus used in this study is shown in Fig. 1. The experimental loop was designed for convective heat transfer in the laminar flow domain. It was constructed with stainless steel tubing, and the fluid was pumped throughout the system by a McMaster-Carr miniature gear pump, part # 8220K43. This pump can operate with a flow rate of 0.61 gal/min (38.5 cm^3/s) at atmospheric pressure and 0.10 gal/min (6.3 cm^3/s) at 20 psi (0.24 MPa). The volumetric flow rate was measured with a FTB9504 Omega flow turbine meter, which has an accuracy of 0.5% in the range of 0.013–0.264 gal/min (0.8–16.7 cm^3/s). The flow meter was positioned just after the pump discharge. The vertical heated section was a stainless steel tube with an inner diameter (ID) of 4.5 mm, outer diameter (OD) of 6.4 mm, and length of 1.01 m. The test section had eight sheathed and electrically insulated T-type thermocouples soldered onto the outer wall of the tubing along axial locations of 5, 16, 30, 44, 58, 89, 100 cm from inlet of the heated section. Two similar T-type thermocouples were inserted into the flow channel before and after the test section to measure the bulk fluid temperatures. These thermocouples and the flow meter provided the data to determine the thermal power of the experimental loop. The test section used in the experiment was resistively heated by a Sorensen DCR 20-125 DC power supply. This power supply has a DC output rating of 0–20 V and current of 125 A. After being heated the fluid was cooled using a chiller that provided flow to a coil placed in the accumulator. The chiller was a Polyscience recirculating chiller, model #1175P. After the test fluid was cooled, it ran through a 1.45 m long and 5.8 mm ID vertical isothermal section where the pressure loss was measured by an Omega PX 154-001DI pressure transducer, able to read up to 1 in. (2.54 cm) of water with an accuracy of 1% of the full scale. A HP3852A data acquisition system controlled by a Visual Basic program was used to record the output of all instrumentation. Additional loop components included a needle valve to control the flow rate throughout the loop and a drain valve. The heated section is insulated to minimize heat loss. The thermal power was compared to the electrical power to determine heat loss during each run. At lower flow rates, the heat loss was found to be higher at >10% and often resulted in larger errors in heat transfer coefficient. These experimental data are therefore not reported in this paper.

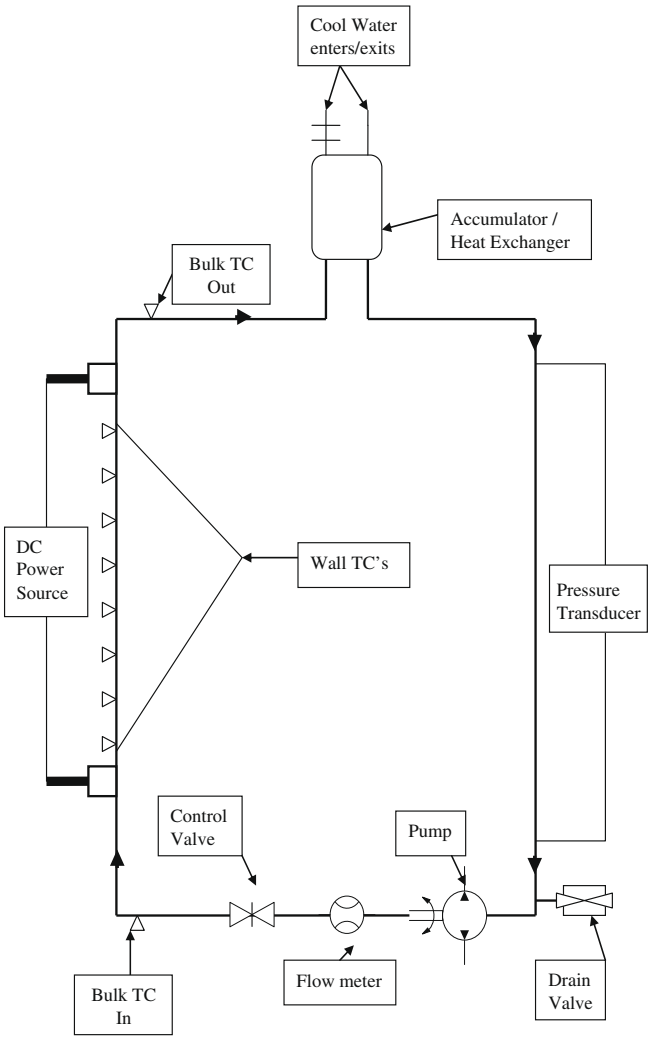

Fig. 1. Schematic of the laminar flow loop.

The coolant temperature ranges from 20 to 37 °C with a temperature rise in the heated section of about 10 °C. The flow velocity ranges from 0.05 to 0.8 m/s. Initial tests were conducted with deionized water for experiment validation.

3. Nanofluid properties

The nanofluids used in this experiment were colloidal alumina and zirconia at 20 wt% (6 vol %) and 12.8 wt% (3 vol %), respectively. These nanofluids were purchased from Nyacol® Nano Technologies Inc. and have a vendor-specified particle size of about 50 nm. These nanofluids were used as-received except for dilution using deionized water. Elemental analysis was performed previously to assure the constituent and the particle weight percent were as specified by the vendor. Full characterization of Nyacol® alumina and zirconia nanofluids such as particle sizing, dispersion stability after dilution was carried out previously to ensure that the stability of the nanofluid was not affected by dilution [23]. Changes of the particle size after dilution are measured to be less than 15 nm which is within the measurement uncertainty (±20 nm) of dynamic-light-scattering [23]. The exact loading of the diluted samples before and after the flow experiments was measured with Inductively Coupled Plasma spectroscopy (ICP). The relative difference in nanofluid concentrations before and after experiments is within 2% which indicated no settling in the loop. Verification tests with deionized water were performed between alumina and zirconia experiments to ensure loop performance was not affected by residual nanoparticles remained in the loop. Characterization was done to assure the specifications of the colloids are as stated by the manufacturer. Detailed information on characterization of these nanofluids can be found in Ref. [22].

The key parameters for assessing the heat transfer merits of nanofluids are their thermophysical properties. The mixture properties of nanofluids are normally expressed in volume percent (ϕ) while the loading analysis was obtained in weight percent (w). The conversion between weight and volume fraction was done through the bulk density (ρ_p).

$$\phi = \frac{w\rho_f}{\rho_p(1-w)+w\rho_f} \tag{1}$$

The density of the nanofluids is by definition:

$$\rho = \phi\rho_p + (1-\phi)\rho_f \tag{2}$$

Assuming thermal equilibrium between the particles and the surrounding fluid, the specific heat is estimated as follows:

$$c = \frac{\phi\rho_p c_p + (1-\phi)\rho_f c_f}{\rho} \tag{3}$$

Specific heats of 880 J/kg K for alumina and 418 J/kg K for zirconia are adopted from the NIST database. The bulk densities for alumina and zirconia are 3920 and 5600 kg/m^3, respectively.

The temperature- and loading-dependent thermal conductivities for the alumina and zirconia nanofluids tested in this study were measured with a short transient hot wire apparatus which was validated with various fluids at different temperatures and found to have ±2% accuracy [24]. The transient hot wire apparatus made use of a teflon-coated platinum wire to prevent the occurrence of parasitic currents in the test fluid. The dependence of thermal conductivity on loading was measured for each fluid from zero to the maximum loading. Temperature dependence of the conductivity was measured from 20 to 80 °C. The measurements show that the loading dependence of thermal conductivity is bracketed by the Maxwell-Garnet model, while the temperature dependence is the same as that of water. Viscosity was measured by a capillary viscometer submerged in a temperature-controlled bath. The viscometer was benchmarked with water at various temperatures and its accuracy was found to be within 0.5%.

Curve fits created for the thermal conductivity and viscosity experimental data were initially reported in Ref. [22]. Since the vendor adopted a new synthesis method for zirconia nanofluid used in this study, its viscosity was re-measured for the current study. The curve fits used in this study are given as follows.

Alumina–water nanofluid

$$k(\phi,T) = k_f(T)(1+4.5503\phi) \tag{4}$$

$$\mu(\phi,T) = \mu_f(T)\exp[4.91\phi/(0.2092-\phi)] \tag{5}$$

Zirconia–water nanofluid

$$k(\phi,T) = k_f(T)(1+2.4505\phi-29.867\phi^2) \tag{6}$$

$$\mu(\phi,T) = \mu_f(T)(1+46.801\phi+550.82\phi^2) \tag{7}$$

The applicable temperature range of these equations is 20 °C < T < 80 °C, with volumetric loadings up to 6% for alumina and up to 3% for zirconia.

4. Results and discussion

4.1. Heat transfer characteristics

The heat transfer coefficient, h, was derived as follows:

$$h = \frac{q''}{T_{wi}-T_b}$$

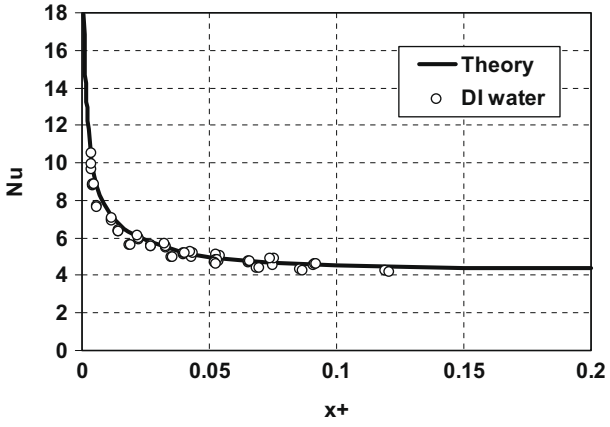

Fig. 2. Measured Nusselt numbers versus x^+ for deionized water.

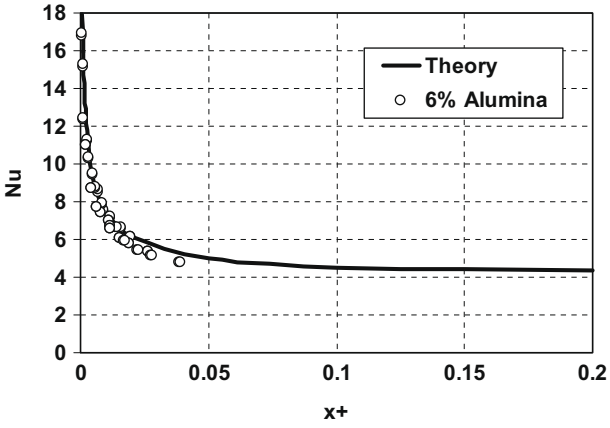

Fig. 3. Measured Nusselt numbers versus x^+ for 6 vol % alumina nanofluid.

where q'' is the heat flux on the tube inner wall, T_{wi} is the inner wall temperature, and T_b is the calculated bulk temperature at the axial location of interest. The heat flux is determined from knowledge of the test section thermal power and geometry. The inner wall temperature is calculated using the analytical solution of the conduction equation with the measured outer wall temperature as the boundary condition and the temperature-dependent thermal resistance of the stainless steel wall. The outer wall temperatures are measured at various axial locations along the heated section. Temperature-dependent thermal physical properties of the nanofluids are used in the heat transfer coefficient and dimensionless number calculations based on the local bulk coolant temperature.

To allow comparison with theory, we adopted the following curve fits which reproduce the complicated analytical solution for local Nusselt number to within 1% discrepancy [25]:

$$Nu = 1.302\left(\frac{x^+}{2}\right)^{-1/3} - 0.5, \quad x^+ \leqslant 0.003 \tag{8}$$

$$Nu = 4.364 + 0.263\left(\frac{x^+}{2}\right)^{-0.506} e^{-41(x^+/2)}, \quad x^+ > 0.003$$

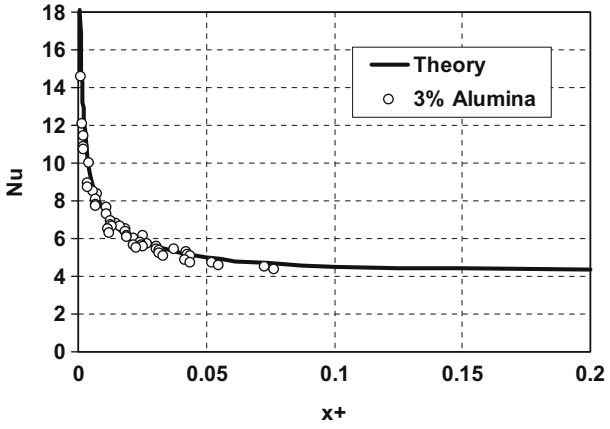

Fig. 4. Measured Nusselt numbers versus x^+ for 3 vol % alumina nanofluid.

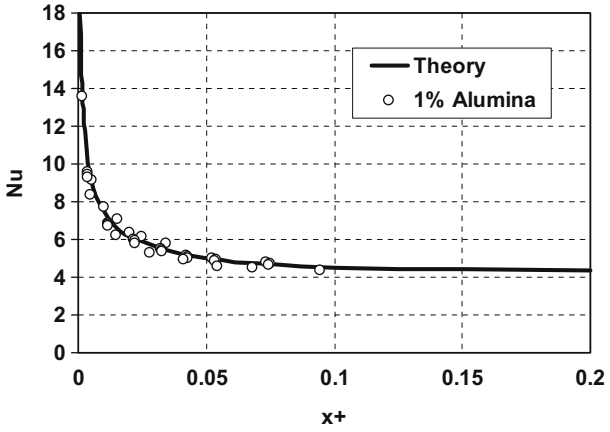

Fig. 5. Measured Nusselt numbers versus x^+ for 1 vol % alumina nanofluid.

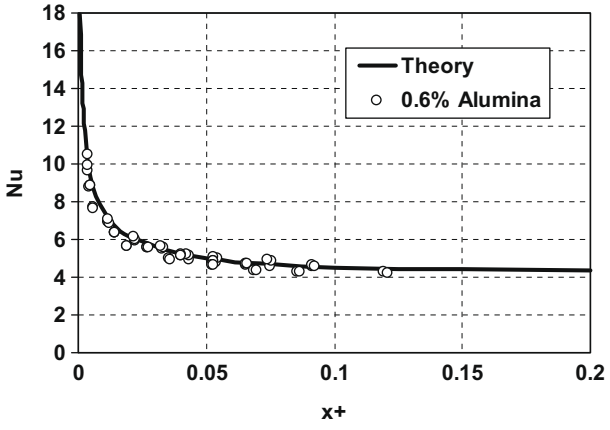

Fig. 6. Measured Nusselt numbers versus x^+ for 0.6 vol % alumina nanofluid.

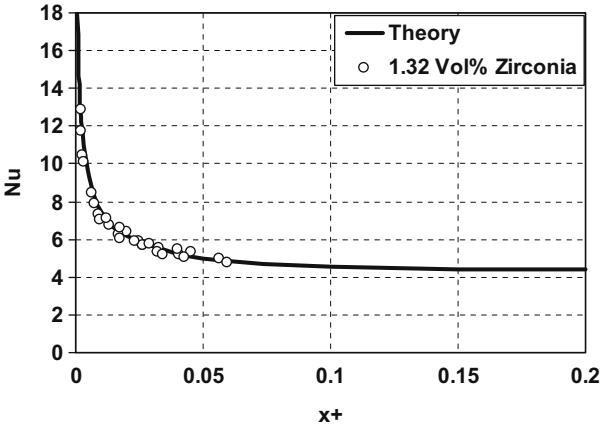

Fig. 7. Measured Nusselt numbers versus x^+ for 1.32 vol % zirconia nanofluid.

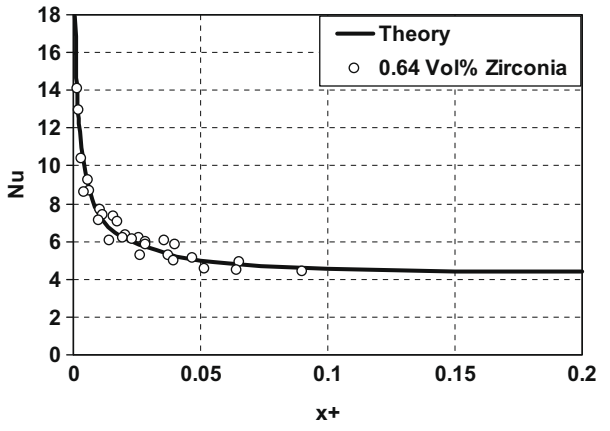

Fig. 8. Measured Nusselt numbers versus x^+ for 0.64 vol % zirconia nanofluid.

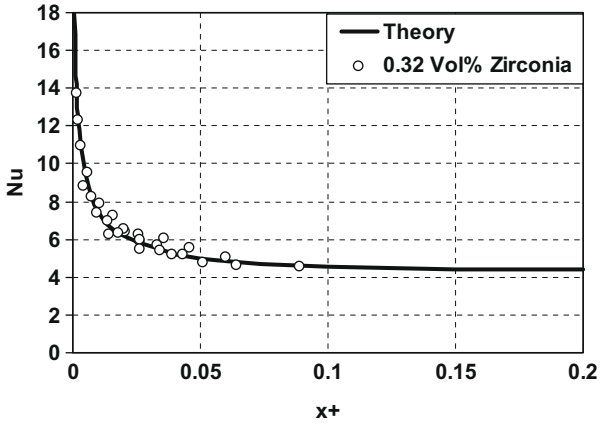

Fig. 9. Measured Nusselt numbers versus x^+ for 0.32 vol % zirconia nanofluid.

where $Nu = \frac{hD}{k}$.

The dimensionless distance is defined as:

$$x^+ = \frac{2(x/D)}{RePr} \tag{9}$$

Re is the Reynolds number $Re = \frac{\rho VD}{\mu}$ and Pr is the Prandtl number $Pr = \frac{c\mu}{k}$.

Initial tests with deionized water confirmed that the heat transfer coefficients were as predicted for laminar flow in a round channel with constant heat flux, as shown in Fig. 2. The measurements are within 10% of prediction. This result confirms that the loop is working properly. The experimental results for nanofluids are also compared against the theory (Eq. (8)) based on the dimensionless numbers Nu and x^+. This enables the evaluation of nanofluid heat transfer performance on the basis of their respective properties. The temperature- and loading- dependent properties of the fluid as described in Section 3 are used to derive these numbers.

The alumina nanofluid data for the four different volumetric loadings (0.6%, 1%, 3% and 6%) are shown in Figs. 3–6. The Nusselt numbers are in good agreement with the theory prediction, if the mixture properties are utilized for alumina nanofluid.

The zirconia nanofluid data at three volumetric loadings (0.32%, 0.64%, and 1.32%) are shown in Figs. 7–9. The data points are again in good agreement with prediction, if the measured mixture properties of the zirconia nanofluid are used. The experimental data for water and nanofluids are also listed in Table 1.

Table 1
Experimental data for laminar heat transfer coefficient in water and nanofluids.

ϕ	Flow rate (gpm)	T_{in} (°C)	T_{out} (°C)	Re	h_1	h_2	h_3	h_4	h_5	h_6	h_7
0	0.0495	26.51	36.71	1035	1434.59	954.51	815.46	756.13	685.68	663.20	636.34
0	0.0485	21.82	30.49	937	1305.23	935.80	818.29	756.87	706.30	688.99	672.85
0	0.0498	21.79	36.71	976	1346.81	956.57	833.87	775.34	718.83	700.68	678.79
0	0.0402	22.06	30.98	780	1193.55	860.57	754.93	699.70	655.31	640.27	627.75
0	0.0401	21.85	31.47	780	1202.92	868.62	763.46	708.95	665.36	651.31	640.54
0	0.0398	21.89	31.56	775	1196.10	864.93	760.28	705.15	663.13	648.97	636.23
0	0.0308	22.04	31.90	601	1048.41	768.08	681.17	636.32	601.83	591.81	588.72
0	0.0304	21.89	32.34	595	1039.29	762.21	675.87	631.72	597.93	588.26	582.68
Alumina–water nanofluid											
0.0065	0.1012	21.72	31.98	1797	2002.70	1359.21	1142.95	1014.73	918.79	878.46	832.18
0.0065	0.1027	20.60	30.51	1762	1906.02	1314.08	1115.28	983.83	887.81	848.90	801.57
0.0065	0.0506	21.40	31.00	884	1301.06	952.82	834.76	779.74	722.70	701.88	683.38
0.0065	0.0523	21.27	30.54	907	1326.04	968.44	847.49	789.85	730.93	709.90	689.70
0.0065	0.0504	21.33	31.15	881	1311.85	944.95	826.45	771.28	715.46	695.20	674.78
0.0065	0.0403	21.52	31.35	708	1175.92	866.28	766.33	716.94	671.64	655.63	644.22
0.0065	0.0424	21.37	30.68	738	1222.71	893.54	788.99	736.77	688.98	672.13	661.76
0.0065	0.0408	21.36	30.81	710	1197.40	878.31	775.98	725.38	678.51	662.56	653.41
0.0132	0.1085	22.63	31.84	1888	1945.63	1310.87	1110.08	1017.07	917.33	885.32	844.74
0.0132	0.0510	21.73	31.27	870	1363.50	980.93	857.21	791.45	739.95	719.22	698.18
0.0132	0.0500	21.56	32.03	858	1340.32	969.92	846.09	783.65	729.51	709.26	686.93
0.0132	0.0500	21.48	31.39	852	1319.81	955.20	834.29	770.98	719.58	699.70	678.19
0.0132	0.0395	21.73	32.63	685	1190.23	888.91	762.08	708.16	664.92	648.79	632.91
0.0132	0.0420	21.57	31.81	719	1241.70	911.75	801.89	743.55	699.95	683.75	670.65
0.0132	0.0389	21.62	31.77	667	1189.37	868.37	764.11	708.49	667.10	651.91	638.25
0.0132	0.0297	20.84	32.09	505	992.40	747.15	661.43	618.62	582.83	573.04	563.44
0.0132	0.0297	21.18	31.57	504	997.91	757.42	674.41	630.77	598.66	588.81	585.38
0.0132	0.0327	21.49	30.59	551	1055.33	801.31	715.01	667.26	634.67	622.29	620.26
0.0276	0.1513	23.07	32.42	1666	2252.86	1546.14	1300.69	1193.42	1058.83	1019.44	970.62
0.0276	0.1020	22.94	33.15	1131	1858.15	1312.22	1126.02	1031.03	934.47	899.92	854.82
0.0276	0.0903	22.75	32.59	992	1767.05	1252.23	1079.34	986.44	900.31	866.82	825.83
0.0276	0.0895	22.27	30.89	957	1675.08	1206.24	1044.18	954.75	877.12	844.65	804.79
0.0276	0.0871	22.14	30.92	930	1651.47	1188.81	1029.12	941.63	864.63	832.92	794.19
0.0276	0.0526	21.38	31.79	562	1371.59	1003.65	876.42	808.04	756.12	733.65	709.09
0.0276	0.0500	21.58	31.72	535	1336.03	974.72	850.38	783.74	732.95	711.58	687.39
0.06	0.2518	25.62	34.85	1089	2897.67	1936.82	1634.54	1483.30	1312.22	1251.16	1155.64
0.06	0.2528	26.22	36.20	1117	2927.12	1956.51	1648.66	1500.08	1324.07	1262.01	1166.94
0.06	0.2040	25.74	35.69	887	2637.34	1793.95	1519.25	1376.80	1226.54	1168.28	1079.11
0.06	0.2040	25.74	35.69	891	2637.34	1793.95	1519.25	1376.80	1226.54	1168.28	1079.11
0.06	0.1505	25.23	34.31	644	1679.56	1266.11	1106.42	1018.16	931.78	893.47	837.00
0.06	0.1502	25.61	35.78	552	1691.70	1270.06	1111.46	1023.37	934.32	896.50	840.15
0.06	0.1031	24.22	33.36	431	1894.10	1333.10	1139.15	1031.66	939.99	898.69	840.00
0.06	0.1016	24.33	34.79	432	1898.58	1334.28	1138.38	1032.10	940.23	898.51	836.77
Zirconia–water nanofluid											
0.0032	0.1021	22.05	32.62	356	1875.25	1304.33	1083.14	996.60	888.47	867.03	847.33
0.0032	0.0796	21.96	32.87	278	1682.94	1132.30	958.33	900.83	812.48	793.81	775.45
0.0032	0.0610	21.73	33.22	213	1494.33	1015.97	870.85	820.02	744.17	725.06	710.22
0.0032	0.0408	21.05	32.06	140	1205.63	860.70	751.71	710.41	655.97	641.50	633.63
0.0064	0.1020	20.93	34.33	362	1934.62	1278.41	1069.06	1016.21	883.74	867.64	853.07
0.0064	0.0909	22.28	32.80	324	1788.67	1201.79	1024.66	976.25	856.28	839.20	825.69
0.0064	0.0558	21.76	35.56	203	1432.34	987.96	856.44	811.97	734.75	717.97	698.28
0.0064	0.0404	21.16	32.47	141	1182.42	839.26	732.25	692.15	637.88	623.89	617.82
0.0132	0.0792	22.09	33.64	293	1650.35	1119.64	956.87	905.62	808.96	789.71	763.88
0.0132	0.0638	22.09	31.90	231	1469.63	1030.83	889.27	834.35	763.24	742.50	718.09
0.0132	0.0602	21.49	31.92	216	1418.70	988.37	856.73	806.08	735.59	715.74	688.44
0.0132	0.0896	22.02	34.27	333	1816.71	1197.75	1006.59	941.72	846.69	823.05	788.81

h_1 through h_7 are heat transfer coefficients (W/m^2 K) measured at axial locations of 5, 16, 30, 44, 58, 89, 100 cm from inlet of the heated section, respectively.

Next we will discuss the heat transfer performance of nanofluids in the entrance region in some detail. The thermal entry length for laminar flow in a tube with the constant heat flux boundary condition is approximately $\frac{x}{D} \approx 0.04RePr$ [25], corresponding to a dimensionless entrance length $x^+ \approx 0.08$. However, most of the *Nu* variation occurs for $x^+ < 0.01$. The following curve fit is a simplified equation obtained for $x^+ \leqslant 0.01$ from Eq. (8):

$$Nu = 1.619(x^+)^{-1/3} \tag{10}$$

The heat transfer coefficient can be derived from Eq. (10) to obtain the following expression :

$$h \propto \left(\frac{k^2 \rho Vc}{xD}\right)^{1/3} \tag{11}$$

Eq. (11) suggests that, for given velocity, diameter, and axial location, the heat transfer coefficient for the entrance region scales with the fluid properties as follows:

$$h \propto (k^2 \rho c)^{1/3} \tag{12}$$

Using Eq. (12), it is estimated that the heat transfer enhancement for 6 vol % alumina nanofluid and 1.32 vol % zirconia nanofluid in the entrance region are 17% and 2%, respectively.

Fig. 10 shows comparisons of the predicted and experimental ratios of alumina–water and zirconia–water nanofluid heat transfer coefficients to the water heat transfer coefficient in the entrance region. Each data point represents the average of the heat transfer coefficient ratios of nanofluid to water for axial locations corresponding to $x^+ \leqslant 0.01$ at various experiment conditions. As shown in the comparison, there appears to be no abnormal heat transfer enhancement in the entrance region beyond what is predicted based on the mixture thermophysical properties. The error bars represents ±10% as indicated previously.

It is worthwhile noting that the predictions of alumina and zirconia heat transfer enhancements have distinctively different trends. While the heat transfer enhancement ratio of alumina nanofluid increases with loading, zirconia nanofluid reaches a maximum of about 3% at about 3.5 vol %, because the decreasing specific heat outweighs the slowly increasing thermal conductivity. This underscores the importance of including other thermophysical properties besides thermal conductivity when evaluating the heat transfer performance of nanofluids.

As shown in Eq. (8) for fully developed laminar flow ($x^+ > 0.1$), the Nusselt number approaches a constant value and therefore the heat transfer coefficient is proportional to thermal conductivity. Under these conditions, the estimated heat transfer enhancements for 6 vol % alumina and 1.32 vol % zirconia are 27% and 3%, respectively.

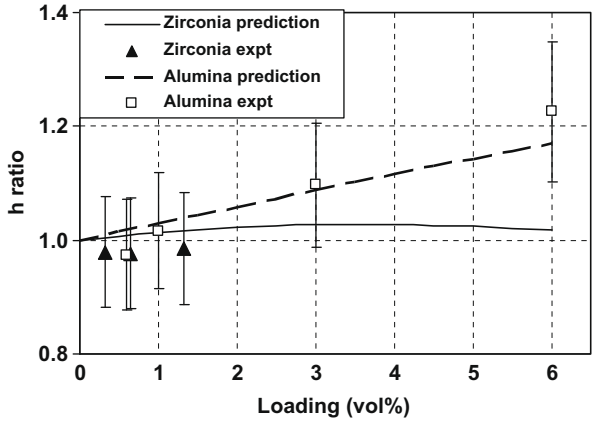

Fig. 10. Heat transfer coefficient ratios of alumina and zirconia nanofluids to water in the entrance region.

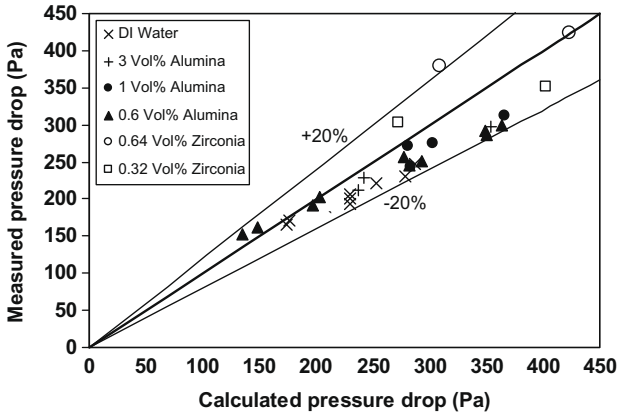

Fig. 11. Comparison of measured and predicted pressure losses for water and nanofluid tests.

4.2. Viscous pressure loss

In conjunction with the heat transfer measurements, the viscous pressure loss was measured in the isothermal section of the loop for water, alumina and zirconia nanofluids. The experimental results were compared with the pressure loss predictions

$$\Delta P = f \frac{L}{D} \frac{\rho V^2}{2} \tag{13}$$

where the friction factor for fully-developed laminar flow in a circular pipe is [25]:

$$f = 64/Re \tag{14}$$

Water results are in good agreements with prediction of Eq. (13). Due to high viscosity, pressure loss of some higher concentration nanofluids exceeded the upper limit of the low-pressure transducer and these test results were not reported here. Fig. 11 compares viscous pressure drops of water, alumina and zirconia nanofluid at various concentrations. The measured viscous pressure losses are within ±20% of predictions. By combining Eq. (13) and (14), it can be seen that, for a given flow velocity and channel geometry, the pressure loss is proportional to viscosity only. As nanofluids tend to have very high viscosity (see Eqs. (5) and (7)), viscous pressure losses can become a significant issue when considering nanofluids for practical applications. For example, at 6 vol % the viscosity of our alumina nanofluid is about 7.2 times higher than that of water, thus resulting in same increase in pressure loss.

5. Conclusions

The heat transfer and viscous pressure loss characteristics of alumina–water and zirconia–water nanofluids in laminar flow regime were studied experimentally. It was found that, for given velocity and channel geometry, 6 vol % alumina nanofluid heat transfer coefficient can be up to 27% higher than that of water in the entrance region, while the zirconia nanofluid heat transfer coefficient displays a much lower enhancement with respect to water. While heat transfer enhancement of alumina increases with loading, zirconia exhibit a maximum enhancement at 3% at 3.5 vol % loading. However, when the data are plotted using dimensionless numbers (*Nu* and x^+), based on the measured properties of the nanofluids, they show good agreement with the predictions of the traditional models/correlations for laminar flow. This suggests that the nanofluids behave as homogeneous mixtures. As such, the heat transfer coefficient enhancement is not abnormal, but simply due to the different mixture properties of the nanofluids with

respect to water. Similar conclusions apply to the pressure loss, i.e., the nanofluid pressure loss is higher than water's, but scales linearly with the fluid viscosity, as expected from the traditional pressure loss theory for laminar flow.

Acknowledgments

The authors thank Dr. Wesley Williams for his assistance with initial design and construction of the flow loop. This project is funded by the Department of Energy Innovation in Nuclear Infrastructure and Education Grant (DOE-FG07-02ID14420).

References

[1] A.S. Ahuja, Augmentation of heat transport in laminar flow of polystyrene suspensions. I. Experiments and results, J. Appl. Phys. 46 (1975) 3408.
[2] K.V. Liu, U.S. Choi, K.E. Kasza, Measurement of pressure drop and heat transfer in turbulent pipe flows of particulate slurries, Argonne National Laboratory Report, ANL-88-15, 1988.
[3] H. Masuda, A. Ebata, K. Teramae, N. Hishinuma, Alteration of thermal conductivity and viscosity of liquid by dispersing ultra-fine particles (dispersion of Al_2O_3, SiO_2, and TiO_2 ultra-fine particles), Netsu Bussei 4 (1993) 227.
[4] S.U.S. Choi, Enhancing thermal conductivity of fluids with nanoparticles, in: D.A. Siginer, H.P. Wang (Eds.), Developments and Applications of Non-Newtonian Flows, American Society of Mechanical Engineers, New York, 1995.
[5] J. Eastman, S.U.S. Choi, S. Li, W. Yu, L.J. Thompson, Anomalously increased effective thermal conductivities of ethylene-glycol-based nanofluids containing copper nanoparticles, Appl. Phys. Lett. 78 (2001) 718–720.
[6] S.U.S. Choi, Z.G. Zhang, W. Yu, F.E. Lockwood, E.A. Grulke, Anomalous thermal conductivity enhancement in nanotube suspensions, Appl. Phys. Lett. 79 (2001) 2252–2254.
[7] M.J. Assael, C.-F. Chen, I. Metaxa, W.A. Wakeham, Thermal conductivity of suspensions of carbon nanotubes in water, Int. J. Thermophys. 25 (2004) 971–985.
[8] J.C. Maxwell-Garnett, Colours in metal glasses and in metallic films, Philos. Trans. R. Soc. Lond. Ser. A 203 (1904) 385–420.
[9] R.L. Hamilton, O.K. Crosser, Thermal conductivity of heterogeneous two-component systems, Indus. Eng. Chem. Fundam. 1 (3) (1962) 187–191.
[10] B.C. Pak, Y.I. Cho, Hydrodynamic and heat transfer study of dispersed fluids with submicron metallic oxide particles, Exp. Heat Transfer 11 (1998) 151.
[11] Y. Xuan, Q. Li, Investigation on convective heat transfer and flow features of nanofluids, J. Heat Transfer 125 (2003) 151–155.
[12] Y. Xuan, W. Roetzel, Conceptions for heat transfer correlation of nanofluids, Int. J. Heat Mass Transfer 43 (2000) 3701–3707.
[13] Y. Yang, Z.G. Zhang, E.A. Grulke, W.B. Anderson, G. Wu, Heat transfer properties of nanoparticle-in-fluid dispersions (nanofluids) in laminar flow, Int. J. Heat Mass Transfer 48 (2005) 1107–1116.
[14] D. Wen, Y. Ding, Experimental investigation into convective heat transfer of nanofluids at the entrance region under laminar flow conditions, Int. J. Heat Mass Transfer 47 (2004) 5181–5188.
[15] Y. Ding, H. Alias, D. Wen, R.A. Williams, Heat transfer of aqueous suspensions of carbon nanotubes (CNT nanofluids), Int. J. Heat Mass Transfer 49 (2006) 240–250.
[16] S.Z. Heris, M.N. Esfahany, G. Etemad, Investigation of CuO/water nanofluid laminar convective heat transfer through a circular tube, J. Enhanced Heat Transfer 13 (2006) 279–289.
[17] S.Z. Heris, M.N. Esfahany, S.Gh. Etemad, Experimental investigation of convective heat transfer of Al_2O_3/water nanofluid in circular tube, Int. J. Heat Fluid Flow 28 (2007) 203–210.
[18] Y. He, Y. Jin, H. Chen, Y. Ding, D. Chang, H. Lu, Heat transfer and flow behaviour of aqueous suspensions of TiO_2 nanoparticles (nanofluids) flowing upward through a vertical pipe, Int. J. Heat Mass Transfer 50 (2007) 2272–2281.
[19] J. Lee, R.D. Flynn, K.E. Goodson, J.K. Eaton, Convective heat transfer of nanofluids (DI water–Al_2O_3) in microchannels, HT2007-32630, ASME-JSME Thermal Engineering Summer Heat Transfer Conference, July 8–12, Vancouver, BC, Canada, 2007.
[20] R. Chein, J. Chuang, Experimental microchannel heat sink performance studies using nanofluids, Int. J. Thermal Sci. 46 (2007) 57–66.
[21] C.T. Nguyen, G. Roy, C. Gauthier, N. Galanis, Heat transfer enhancement using Al_2O_3–water nanofluid for an electronic liquid cooling system, Appl. Thermal Eng. 27 (2007) 1501–1506.
[22] W.C. Williams, J. Buongiorno, L.W. Hu, Experimental investigation of turbulent convective heat transfer and pressure loss of alumina/water and zirconia/water nanoparticle colloids (nanofluids) in horizontal tubes, J. Heat Transfer 130 (2008) 042412.
[23] W.C. Williams, Experimental and theoretical investigation of transport phenomena in nanoparticle colloids (nanofluids), Ph.D. Thesis, Massachusetts Institute of Technology, Cambridge, 2007.
[24] R. Rusconi, W.C. Williams, J. Buongiorno, R. Piazza, L.W. Hu, Numerical analysis of convective instabilities in a transient short-hot-wire setup for measurement of liquid thermal conductivity, Int. J. Thermophys. 28 (2007) 1131–1146.
[25] J.H. Lienhard IV, J.H. Lienhard V, A Heat Transfer Textbook, second ed., Phlogiston Press, 2002.